Phase diagram of charge-stabilized colloidal suspensions: van der Waals instability without attractive forces

René van Roij and Marjolein Dijkstra
H. H. Wills Physics Laboratory, Royal Fort, University of Bristol, Bristol BS8 1TL, United Kingdom

Jean-Pierre Hansen
Department of Chemistry, University of Cambridge, Cambridge CB2 1EW, United Kingdom
(Received 6 October 1998)

A careful analysis of the classic Derjaguin-Landau-Verwey-Overbeek theory of the interaction energy in a suspension of charge-stabilized, spherical colloidal particles (polyions) in the presence of salt shows that in addition to the usual screened-Coulomb effective pair interaction between polyions, there exists a structure-independent but state-dependent contribution (the ''volume'' term), which has almost invariably been overlooked. A variational procedure based on the Gibbs-Bogoliubov inequality is used to calculate the contribution of the polyion pair interactions to the free energy of the suspension. The latter is then combined with the ''volume'' term to derive the phase diagram of the colloidal suspension. Although the effective pair interaction between polyions is purely repulsive, it is shown that the volume term may drive a van der Waals–like instability in highly deionized suspensions (salt concentrations less than 20 μM) for experimentally relevant choices of the polyion radius and charge. If the latter are sufficiently large, the fluid-fluid phase separation is preempted by the fluid-solid freezing transition which broadens considerably. Reentrant behavior is predicted on the solid side of the phase diagram. The predicted phase diagrams may provide an explanation of some surprising recent experimental results. They also show that the observation of a fluid-fluid phase separation in a charge-stabilized colloidal dispersion does not necessarily imply the existence of an attractive component in the effective pair interaction between highly charged polyions. [S1063-651X(99)04002-7]

PACS number(s): 82.70.Dd, 64.10.+h, 83.20.Di, 64.60.Cn

I. INTRODUCTION

Phase separation of an initially homogeneous fluid into dense (or concentrated) and dilute fluid phases is a very common phenomenon in molecular systems. In one-component systems, involving a single molecular species, the separation into liquid and gas phases observed below the critical temperature T_c is attributed, since van der Waals, to intermolecular attractions which balance the loss of configurational entropy upon condensation. In mixtures of two or more components, the mechanism for demixing into phases of different concentrations of the various species is less clear-cut. In the case of molecules of comparable size, the role of attractive interactions is again believed to be preeminent [1], since purely repulsive interactions do not appear to lead to phase separation, as long as they are additive. The situation is more complicated for colloidal suspensions, which are essentially multicomponent in nature and involve large size-asymmetries between the individual species. Such suspensions consist of mesoscopic colloidal particles, a molecular solvent, and most frequently at least one third component, such as polymer coils or microscopic ions, which introduce an intermediate length scale (the radius of gyration R_g for polymers or the Debye screening length λ_D for ions). This third component plays a crucial role, since it induces *effective* interactions between the colloidal particles, which are of largely entropic origin. Effective interactions result quite naturally from a formal contraction of the initial multicomponent system into an effective one-component description involving only the colloidal particles. An important difference with simple molecular systems is that the control parameter is not the temperature but the concentration of the third component. It is worth noting that the solvent is not directly involved in the phase separation mechanism, and plays the role of a passive ''spectator'' phase.

In the case of sterically stabilized colloidal particles, free polymer coils induce a depletion interaction between colloids which is predominantly attractive and of a range of the order of R_g beyond the colloid particle diameter [2,3]. There is ample experimental and theoretical evidence [4–6] that the depletion attraction can induce a liquid-gas separation of the suspension into a high colloid concentration (''liquid'') phase and a dilute (''gas'') phase, at least if the polymer coils are assumed to be ideal (nonadditive). This gas-liquid transition is thus reminiscent of the van der Waals phase transition in ordinary molecular fluids. Recent results indicate, however, that additivity of the pair interactions (such as in an asymmetric binary hard-sphere mixture) tends to drive the gas-liquid transition metastable with respect to freezing [7].

In the present paper, we focus on charge-stabilized colloidal suspensions, made up of highly charged, spherical polyions and microscopic coions and counterions dissolved in water. The microions form electric double layers around the charged surface of the polyions, and it is generally accepted that, at least in the bulk, the effective interactions between electric double layers surrounding different polyions are purely repulsive. Direct measurements [8], as well as first-principles computer simulations [9], point to the quantitative validity of the Derjaguin-Landau-Verwey-Overbeek (DLVO) [10] potential between charge-stabilized colloidal particles, provided an adequate choice is made for the effective charge

of the polyions, which is generally significantly less than the structural charge related to the number of ionizable surface radicals. We shall not consider here the case of confined colloids, where the presence of charged walls has been shown to induce an attractive component to the effective interaction between like-charged polyions [11–13].

According to the classical van der Waals picture, the absence of attractive interactions between polyions in bulk seems to preclude any phase separation into dilute and concentrated (fluid or solid) colloid phases. This picture seems, however, to be contradicted by some experimental results. The relevant experiments are invariably performed at extremely low salt concentration, of the order of a few μM, such that the influence of attractive van der Waals–London dispersion forces may be safely ruled out. In one experiment, the measured lattice spacings in crystalline phases of such quasideionized suspensions were found to be smaller than expected on the basis of a space-filling structure of the known colloid concentration [14]. A natural explanation of this observation would be that the dense crystalline phase is not pure, but coexists with a much more dilute gas phase. More evidence of phase coexistence has been provided by the observation of extremely dilute voids (a gas phase) in the bulk of an apparently homogeneous deionized suspension (a liquid [15] or a solid [12]). In fact, even a fully equilibrated gas-liquid coexistence has been reported [16], although this observation aroused some controversy [17].

There thus appears to be a contradiction between the observation of the coexistence of dilute and concentrated phases and the generally accepted view of a purely repulsive effective interaction between like-charged polyions. In this paper we carefully reexamine the traditional DLVO theory. We recover an effective screened-Coulomb (or Yukawa) pair interaction, as expected, but in addition the total effective potential energy for any given configuration of the polyions turns out to contain a structure-independent but state-dependent volume term, the existence of which had already been pointed out by Silbert and Grimson [18]. It will be shown that this volume term contributes significantly to the free energy of the polyions, and varies sufficiently rapidly at very low salt concentrations to have a very marked effect on the phase diagram. Under experimentally achievable conditions it leads to complex fluid-fluid-solid phase diagrams when the colloid and salt concentrations are varied. In particular, a van der Waals–like phase separation between dilute and concentrated fluid phases is predicted, despite the purely repulsive nature of the effective pair potential. We believe that the calculation to be presented provides a plausible explanation of experimental observations. The present work supplements and corrects a preliminary version published elsewhere [19].

II. THE MODEL

The colloidal dispersion under consideration is assumed to contain (i) N_p identical spherical polyions of radius R and charge $-Ze$ (uniformly distributed over the particle surface); (ii) $N_c = ZN_p$ identical counterions of charge $+e$; and (iii) N_s fully dissociated pairs of monovalent salt ions of charge $\pm e$. The solvent (water) is assumed to be a continuum of dielectric constant ϵ (''primitive model''), and the total volume is denoted by V. All microions are assumed to be point particles, which cannot penetrate the interior of the spherical polyions. The total numbers of microscopic cations and anions in the suspension are $N_+ = N_c + N_s$ and $N_- = N_s$. The corresponding mean (macroscopic) number density will be denoted by $n_\pm = N_\pm / V$, the total microion density by $n = n_+ + n_-$, and the polyion density by $n_p = N_p / V$.

The above model is characterized by the total Hamiltonian

$$H = H_p + H_m + H_{mp}, \tag{1}$$

where H_p and H_m are the Hamiltonians associated with the polyions and microions, and H_{mp} is the microion-polyion interaction term. For later reference we write the polyion Hamiltonian explicitly as a sum of kinetic and potential energy,

$$H_p = K_p + V_p(\{R_{ij}\}) = K_p + \sum_{i<j}^{N_p} \left[v_0(R_{ij}) + \frac{Z^2 e^2}{\epsilon R_{ij}} \right], \tag{2}$$

where K_p is the kinetic energy and V_p the pairwise potential energy consisting of a hard-sphere contribution $v_0(R_{ij})$ and a Coulombic contribution. Here $R_{ij} = |\mathbf{R}_i - \mathbf{R}_j|$ denotes the separation between polyion i and j, $\mathbf{R}_{i,j}$ being their position vectors, respectively.

Several remarks are in order concerning the model Hamiltonian (1). (a) It contains exclusively short-range excluded volume and long-range Coulombic interactions. Long-range dispersion interactions are omitted. This turns out to be justified, since the low salt concentration regime to be considered later gives rise to weakly screened Coulomb interactions that completely mask the dispersion interactions. The strong screening (high salt concentration) regime was explicitly considered in Ref. [20], where it was shown that the van der Waals–London-Hamaker attraction between the polyions may indeed lead to a van der Waals phase separation. (b) Stability of the system against classical Coulomb collapse requires, strictly speaking, all ions to have finite hard cores. However, the mean-field density-functional formalism adopted later on allows microions to be point ions without causing any divergences. (c) The total Hamiltonian (1) admits a proper thermodynamic limit, despite the infinite range of the Coulomb interactions, because the colloidal system is globally charge-neutral. This is no longer true when manipulating each of the three terms separately because the polyion and microion components are not separately charge-neutral. This difficulty may be overcome by adding compensating uniform backgrounds of opposite charge density, as is done in the theory of liquid metals, considered as two-component ion-electron fluids [21]. An alternative, but equivalent, procedure which will be adopted implicitly throughout this paper is to replace the bare Coulomb interaction $e^2/\epsilon r$ by a screened Coulomb interaction

$$\frac{e^2}{\epsilon r} \rightarrow \frac{e^2}{\epsilon r} e^{-\lambda r} \tag{3}$$

and going to the limit $\lambda \rightarrow 0$ at the end of the calculation, after the thermodynamic limit has been taken.

At fixed inverse temperature $\beta=1/k_BT$, the Helmholtz free energy F of the colloidal suspension may be formally expressed as

$$\exp[-\beta F]=\mathrm{Tr}_p\mathrm{Tr}_m\exp[-\beta H]\equiv\mathrm{Tr}_p\exp[-\beta H_p^{\mathrm{eff}}], \quad (4)$$

where the traces Tr_p and Tr_m denote canonical phase-space integrals over the polyion and microion degrees of freedom. The effective polyion Hamiltonian H_p^{eff} is defined as

$$H_p^{\mathrm{eff}}=H_p+F'\equiv K_p+V_p^{\mathrm{eff}}(\{\mathbf{R}_i\}), \quad (5)$$

where F' is given by

$$\exp[-\beta F']=\mathrm{Tr}_m\exp[-\beta(H_m+H_{mp})]. \quad (6)$$

Clearly, F' may be interpreted as the Helmholtz free energy of an *inhomogeneous* fluid of microions in the *external* field of polyions at fixed positions $\mathbf{R}_i$. Consequently, it depends parametrically on the polyion positions, and the potential energy of the effective one-component system of polyions, already introduced in Eq. (5), is given by

$$V_p^{\mathrm{eff}}(\{\mathbf{R}_i\})=V_p(\{\mathbf{R}_i\})+F'(\{\mathbf{R}_i\}). \quad (7)$$

The above reduction of the initial polyion-microion system to an effective one-component polyion system shows that the latter interact via an effective potential energy that consists of a contribution V_p, given by Eq. (2) as a sum of pair interactions, and the microion-induced contribution F', which is state-dependent and not, *a priori*, pairwise additive.

III. DENSITY-FUNCTIONAL THEORY

A. Formulation

The inhomogeneous distribution of microscopic cations and anions in the external field of the polyions is characterized by equilibrium density profiles $\rho_+(\mathbf{r})$ and $\rho_-(\mathbf{r})$, which are the fundamental quantities in density-functional theory (DFT) [22]. This theoretical framework is based on the existence of a free-energy functional $\mathcal{F}[\rho_+^{(1)},\rho_-^{(1)}]$ of variational density profiles $\rho_\pm^{(1)}(\mathbf{r})$. The equilibrium profiles $\rho_\pm(\mathbf{r})$ must satisfy the Euler-Lagrange or stationarity condition

$$\left(\frac{\delta\mathcal{F}[\rho_+^{(1)},\rho_-^{(1)}]}{\delta\rho_\pm^{(1)}(\mathbf{r})}\right)\Bigg|_{\rho_\pm^{(1)}(\mathbf{r})=\rho_\pm(\mathbf{r})}=\mu_\pm, \quad (8)$$

where, within the canonical formulation, the Lagrange multipliers $\mu_\pm$ must be chosen such as to satisfy the normalization conditions

$$\int_V d\mathbf{r}\rho_\pm(\mathbf{r})=N_\pm. \quad (9)$$

The corresponding equilibrium value of the Helmholtz free energy F' is then given by

$$F'=\mathcal{F}[\rho_+,\rho_-]. \quad (10)$$

It is customary to split the functional $\mathcal{F}$ into ideal gas, external field, Coulomb interaction, and correlation terms [22],

$$\mathcal{F}=\mathcal{F}_{\mathrm{id}}+\mathcal{F}_{\mathrm{ext}}+\mathcal{F}_{\mathrm{Coul}}+\mathcal{F}_{\mathrm{corr}}. \quad (11)$$

The ideal gas contributions can be written down explicitly as

$$\mathcal{F}_{\mathrm{id}}=k_BT\sum_{\alpha=\pm}\int d\mathbf{r}\rho_\alpha^{(1)}(\mathbf{r})[\ln(\rho_\alpha^{(1)}(\mathbf{r})\Lambda_\alpha^3)-1], \quad (12)$$

where Λ_α is the thermal wavelength of microion species $\alpha=\pm$. The external field contribution may be cast into the form

$$\mathcal{F}_{\mathrm{ext}}=\sum_{\alpha=\pm}\int d\mathbf{r}\rho_\alpha^{(1)}(\mathbf{r})U_\alpha(\mathbf{r}), \quad (13)$$

where the external potentials $U_\alpha(\mathbf{r})$, due to the polyions, are multicentered sums

$$U_\pm(\mathbf{r})=\sum_{j=1}^{N_p}u_\pm(\mathbf{r}-\mathbf{R}_j) \quad (14)$$

over the polyion-microion pair interactions $u_\pm(\mathbf{r})$, given by

$$u_\pm(\mathbf{r})=\begin{cases}\mp\dfrac{Ze^2}{\epsilon}\dfrac{1}{r}, & r>R\\[2ex] \mp\dfrac{Ze^2}{\epsilon}\dfrac{1\mp\gamma_\pm}{R}, & r<R.\end{cases} \quad (15)$$

These polyion-microion pair interactions are thus purely Coulombic beyond the polyion core radius R, and chosen to be constant inside the core region. Within an *exact* density functional $\mathcal{F}$, the most relevant choice for the constants $\gamma_\pm$ would be the hard-core limit $\gamma_\pm\to\infty$, ensuring that the microions are excluded from the polyion cores. However, within the framework of the *approximate* functional adopted below, which allows an analytic solution of the stationarity conditions (8), the excluded volume condition will be satisfied for finite values of γ_+ and γ_- to be determined later on. The choice of $u_\pm(\mathbf{r})$ for $r<R$ is reminiscent of ion-electron ''pseudopotentials'' widely used in the theory of metals [21]. A polyion-microion pseudopotential has also been used in a first-principles simulation of charge-stabilized colloids [9], but for different technical reasons.

The mean-field contribution to the microion-microion Coulomb interaction term in the free-energy functional is of the familiar Hartree form

$$\mathcal{F}_{\mathrm{Coul}}=\frac{e^2}{2\epsilon}\int d\mathbf{r}\int d\mathbf{r}'[\rho_+^{(1)}(\mathbf{r})-\rho_-^{(1)}(\mathbf{r})]\times\frac{1}{|\mathbf{r}-\mathbf{r}'|}[\rho_+^{(1)}(\mathbf{r}')-\rho_-^{(1)}(\mathbf{r}')]. \quad (16)$$

To conclude the specification of the functional $\mathcal{F}$, the following two approximations are made: (a) The correlation contribution to the interaction term is neglected, i.e.,

$$\mathcal{F}_{\mathrm{corr}}=0. \quad (17)$$

This mean-field approximation corresponds to a multicentered Poisson-Boltzmann theory for the density profiles

$\rho_{\pm}(\mathbf{r})$ which can only be handled numerically. (b) In order to obtain an analytically tractable theory, the ideal gas contributions (12) are expanded to quadratic order in the local inhomogeneities,

$$\Delta\rho_{\pm}^{(1)}(\mathbf{r})=\rho_{\pm}^{(1)}(\mathbf{r})-n_{\pm}. \tag{18}$$

In view of the constraints (9), this leads to the following approximate expression for the ideal gas contribution to the functional:

$$\mathcal{F}_{\mathrm{id}}\simeq\sum_{\alpha=\pm}\left(F_{\mathrm{id}}(V,T,n_{\alpha})+\frac{k_BT}{2n_{\alpha}}\int d\mathbf{r}(\Delta\rho_{\alpha}^{(1)}(\mathbf{r}))^2\right), \tag{19}$$

where $F_{\mathrm{id}}(V,T,n_{\alpha})=Vk_BTn_{\alpha}[\ln(n_{\alpha}\Lambda_{\alpha}^3)-1]$ is the homogeneous ideal gas contribution from ionic species $\alpha=\pm$.

B. Diagonalization

The free-energy functional to be used in this paper is now defined by Eqs. (11), (13), (16), (17), and (19); it is *quadratic* in the density profiles $\rho_{\pm}^{(1)}(\mathbf{r})$. This suggests diagonalizing the functional $\mathcal{F}$ by changing from the variational fields $\rho_{\pm}^{(1)}(\mathbf{r})$ to their linear combinations

$$\begin{aligned}\rho^{(1)}(\mathbf{r})&=\rho_{+}^{(1)}(\mathbf{r})-\rho_{-}^{(1)}(\mathbf{r}),\\ \sigma^{(1)}(\mathbf{r})&=\frac{n_{-}\rho_{+}^{(1)}(\mathbf{r})+n_{+}\rho_{-}^{(1)}(\mathbf{r})}{n_{+}+n_{-}}.\end{aligned} \tag{20}$$

Clearly, $\rho^{(1)}(\mathbf{r})$ is the local microion charge density in units of e. In the limit of high salt concentration (such that $n_{+}\simeq n_{-}$), $\sigma^{(1)}(\mathbf{r})$ reduces to one-half of the local total microion number density. At lower salt concentrations, however, the physical meaning of $\sigma^{(1)}(\mathbf{r})$ is less obvious; it vanishes if $n_s=0$. The quadratic functional $\mathcal{F}$ is diagonal in the new fields defined in Eq. (20), and can be written as

$$\begin{aligned}\mathcal{F}[\rho^{(1)},\sigma^{(1)}]=&F_{\mathrm{id}}(V,T,n_{+})+F_{\mathrm{id}}(V,T,n_{-})\\&+\mathcal{F}_{\mathrm{el}}[\rho^{(1)}]+\mathcal{F}_{\mathrm{hc}}[\sigma^{(1)}],\end{aligned} \tag{21}$$

where the ''electrostatic'' functional is of the form

$$\begin{aligned}\mathcal{F}_{\mathrm{el}}[\rho^{(1)}]=&\frac{k_BT}{2(n_{+}+n_{-})}\int d\mathbf{r}[\rho^{(1)}(\mathbf{r})-\overline{\rho}]^2\\&+\int d\mathbf{r}\rho^{(1)}(\mathbf{r})U(\mathbf{r})\\&+\frac{e^2}{2\epsilon}\int d\mathbf{r}\int d\mathbf{r}'\frac{\rho^{(1)}(\mathbf{r})\rho^{(1)}(\mathbf{r}')}{|\mathbf{r}-\mathbf{r}'|},\end{aligned} \tag{22}$$

while the ''hard-core'' functional reads

$$\begin{aligned}\mathcal{F}_{\mathrm{hc}}[\sigma^{(1)}]=&\frac{k_BT}{2}\left(\frac{1}{n_{+}}+\frac{1}{n_{-}}\right)\int d\mathbf{r}[\sigma^{(1)}(\mathbf{r})-\overline{\sigma}]^2\\&+\int d\mathbf{r}\sigma^{(1)}(\mathbf{r})W(\mathbf{r}).\end{aligned} \tag{23}$$

In Eqs. (22) and (23), $\overline{\rho}$ and $\overline{\sigma}$ are the macroscopic spatial averages of the variational fields

$$\overline{\rho}=n_{+}-n_{-}=Zn_p, \tag{24}$$

$$\overline{\sigma}=\frac{2n_{+}n_{-}}{n_{+}+n_{-}}=\frac{2n_{+}n_{-}}{n}, \tag{25}$$

while $U(\mathbf{r})$ and $W(\mathbf{r})$ are the following linear combinations of the external fields (14):

$$\begin{aligned}U(\mathbf{r})&=\frac{n_{+}U_{+}(\mathbf{r})-n_{-}U_{-}(\mathbf{r})}{n}\equiv\sum_{j=1}^{N_p}u(\mathbf{r}-\mathbf{R}_j),\\ W(\mathbf{r})&=U_{+}(\mathbf{r})+U_{-}(\mathbf{r})\equiv\sum_{j=1}^{N_p}w(\mathbf{r}-\mathbf{R}_j).\end{aligned} \tag{26}$$

This multicentered character of $U(\mathbf{r})$ and $W(\mathbf{r})$ follows directly from Eq. (14), and the functional form of $u(r)$ and $w(r)$ from the appropriate linear combinations of Eq. (15), which yields with Eq. (26)

$$u(\mathbf{r})=\begin{cases}-\dfrac{Ze^2}{\epsilon}\dfrac{1}{r}, & r>R\\[2ex] -\dfrac{Ze^2}{\epsilon}\dfrac{1-\gamma}{R}, & r<R,\end{cases} \tag{27}$$

$$w(\mathbf{r})=\begin{cases}0, & r>R\\ w_0, & r<R,\end{cases} \tag{28}$$

where the yet undetermined parameters γ and w_0 are given by $\gamma=(n_{+}\gamma_{+}-n_{-}\gamma_{-})/n$ and $w_0=Ze^2(\gamma_{+}+\gamma_{-})/\epsilon R$. Note that both external fields $U(\mathbf{r})$ and $W(\mathbf{r})$ are constant within the cores of the colloidal particles. $U(\mathbf{r})$ is Coulombic outside the cores, while $W(\mathbf{r})$ vanishes there. Thanks to the diagonalization of the quadratic free-energy functional $\mathcal{F}$, the Euler-Lagrange equations (8) reduce to a set of two uncoupled equations for $\rho(\mathbf{r})$ and $\sigma(\mathbf{r})$, or equivalently for the local deviations

$$\Delta\rho(\mathbf{r})=\rho(\mathbf{r})-\overline{\rho}, \tag{29}$$

$$\Delta\sigma(\mathbf{r})=\sigma(\mathbf{r})-\overline{\sigma}. \tag{30}$$

We study these two uncoupled equations separately below.

C. Minimization of $\mathcal{F}_{\mathrm{hc}}$

The ''hard-core'' part of the functional (21) satisfies the stationarity condition

$$\left(\frac{\delta\mathcal{F}_{\mathrm{hc}}[\sigma^{(1)}]}{\delta\sigma^{(1)}(\mathbf{r})}\right)\Bigg|_{\sigma^{(1)}(\mathbf{r})=\sigma(\mathbf{r})}=\mu_{\sigma}, \tag{31}$$

which is easily solved with the result

$$\Delta\sigma(\mathbf{r})=\left(\frac{n_{+}n_{-}}{nk_BT}\right)[\mu_{\sigma}-W(\mathbf{r})]. \tag{32}$$

The Lagrange multiplier μ_σ follows from the normalization condition and reads

$$\mu_\sigma = \eta w_0, \tag{33}$$

where we defined the colloid packing fraction

$$\eta = \frac{4\pi R^3}{3} n_p. \tag{34}$$

The constant w_0 will now be adjusted to satisfy the hard-core condition of zero density within the core and constant outside. It follows from Eqs. (25) and (32) that

$$\sigma(\mathbf{r}) = \overline{\sigma}\left[1 + \frac{1}{2k_BT}\left(\eta w_0 - \sum_{j=1}^{N_p} w(\mathbf{r}-\mathbf{R}_j)\right)\right], \tag{35}$$

which reduces to a multicentered sum of Heaviside step functions $\Theta(x)$,

$$\sigma(\mathbf{r}) = \frac{\overline{\sigma}}{1-\eta} \sum_{j=1}^{N_p} \Theta(|\mathbf{r}-\mathbf{R}_j| - R), \tag{36}$$

provided we set

$$\beta w_0 = \frac{2}{1-\eta}. \tag{37}$$

The resulting hard-core contribution $F'_{\rm hc}$ to the colloid free energy follows from evaluation of $\mathcal{F}_{\rm hc}[\sigma]$ and reads

$$F'_{\rm hc} = k_BT \frac{Vn_+n_-}{n}\left(2 - \frac{1}{2}\beta w_0(1-\eta)\right)\eta w_0 = k_BT \frac{V\eta\overline{\sigma}}{1-\eta}. \tag{38}$$

Note that the equilibrium profile given in Eq. (36) does not, strictly speaking, satisfy the hard-core condition, in the sense that the spherically symmetric profile centered about polyion i gives rise to a nonvanishing density within the core of another polyion $j \neq i$. This problem is inherently connected to the expansion of the functional to quadratic order in the profiles: the resulting stationarity equations give a linear relation between the profile and the multicentered external field, which is unphysical for hard-core interactions. The specific choice for w_0 given in Eq. (37) is, in that sense, the best one within a quadratic functional or a linearized Poisson-Boltzmann theory. A similar problem will be encountered in the minimization of $\mathcal{F}_{\rm el}$.

D. Minimization of $\mathcal{F}_{\rm el}$

The Euler-Lagrange equation associated with the electrostatic part (22) of the functional $\mathcal{F}$ reduces to

$$\mu_\rho = \left.\left(\frac{\delta \mathcal{F}_{\rm el}[\rho^{(1)}]}{\delta \rho^{(1)}(\mathbf{r})}\right)\right|_{\rho^{(1)}(\mathbf{r})=\rho(\mathbf{r})} = \frac{k_BT}{n}\Delta\rho(\mathbf{r}) + \overline{U} + \Delta U(\mathbf{r}) + \frac{e^2}{\epsilon}\int d\mathbf{r}' \frac{\overline{\rho} + \Delta\rho(\mathbf{r}')}{|\mathbf{r}-\mathbf{r}'|}, \tag{39}$$

where $\overline{U}$ denotes the volume average of $U(\mathbf{r}) = \overline{U} + \Delta U(\mathbf{r})$, and where μ_ρ is a Lagrange multiplier. Care must be exercised in handling Eq. (39) in the thermodynamic limit, since both $\overline{U}$ and the Coulomb integral involve divergent volume integrals of the Coulomb potential. The two divergences cancel, but a proper evaluation of the remaining finite constant is most easily achieved by the use of the screened Coulomb potential (3) and the subsequent limiting procedure $\lambda \to 0$. Substitution of the screened for the bare Coulomb potential transforms Eq. (39) into

$$\mu_\rho = \frac{k_BT}{n}\Delta\rho(\mathbf{r}) + U^{(\lambda)}(\mathbf{r}) + \frac{e^2}{\epsilon}\int d\mathbf{r}' \frac{\exp(-\lambda|\mathbf{r}-\mathbf{r}'|)}{|\mathbf{r}-\mathbf{r}'|}[\overline{\rho} + \Delta\rho(\mathbf{r}')], \tag{40}$$

where

$$U^{(\lambda)}(\mathbf{r}) = \sum_{j=1}^{N_p} u^{(\lambda)}(\mathbf{r}-\mathbf{R_j}) \tag{41}$$

is a multicentered sum over the modified polyion-microion pseudopotential

$$u^{(\lambda)}(r) = \begin{cases} -\dfrac{Ze^2}{\epsilon}\dfrac{\exp(-\lambda r)}{r}, & r > R \\ -\dfrac{Ze^2}{\epsilon}\dfrac{\exp(-\lambda R)}{R}(1-\gamma), & r < R. \end{cases} \tag{42}$$

We now introduce the Fourier transform

$$f_{\mathbf{k}} = \int_V d\mathbf{r} f(\mathbf{r}) \exp(i\mathbf{k}\cdot\mathbf{r}) \tag{43}$$

of an arbitrary function $f(\mathbf{r})$ defined in a finite volume with periodic boundary conditions. Fourier transforming Eq. (40) yields

$$\beta\mu_\rho(2\pi)^3\delta(\mathbf{k}) = \frac{1}{n}\Delta\rho_{\mathbf{k}} + \beta U^{(\lambda)}_{\mathbf{k}} + \frac{4\pi l}{(k^2+\lambda^2)}[(2\pi)^3\overline{\rho}\delta(\mathbf{k}) + \Delta\rho_{\mathbf{k}}], \tag{44}$$

where $l = \beta e^2/\epsilon$ is the Bjerrum length, and with the Dirac δ

$$\delta(\mathbf{k}) = \frac{1}{(2\pi)^3}\int_V d\mathbf{r} \exp(i\mathbf{k}\cdot\mathbf{r}). \tag{45}$$

Now μ_ρ is determined by the normalization (9), which involves the $\mathbf{k}=\mathbf{0}$ Fourier component

$$\Delta\rho_{\mathbf{k}=0}=0. \tag{46}$$

If we use that $(2\pi)^3\delta(\mathbf{k}=0)=V$, Eq. (46) implies

$$\beta\mu_\rho=\frac{1}{V}\,\beta U^{(\lambda)}_{\mathbf{k}=0}+\frac{4\pi l\overline{\rho}}{\lambda^2}. \tag{47}$$

The explicit solution of the stationarity condition (44) now reads

$$\Delta\rho_{\mathbf{k}}=-n\frac{k^2+\lambda^2}{k^2+\kappa_\lambda^2}\beta U^{(\lambda)}_{\mathbf{k}}+\frac{(2\pi)^3\delta(\mathbf{k})}{V}n\frac{\lambda^2}{\kappa_\lambda^2}\beta U^{(\lambda)}_{\mathbf{k}=0}, \tag{48}$$

where we defined the Debye screening parameter $\kappa=\lambda_D^{-1}$ given by

$$\kappa^2=4\pi ln \tag{49}$$

and its modified counterpart $\kappa_\lambda^2=\kappa^2+\lambda^2$. Clearly, κ_λ reduces to κ when the limit $\lambda\to 0$ is taken at the end of the calculation. It is essential to substitute the solution (48) into the Coulombic part of the functional to calculate the contribution to the equilibrium free energy before taking the $\lambda\to 0$ limit (cf. the following section and Appendix A). However, the form of the charge-density profile in that limit can be directly obtained by Fourier transforming the solution (48) at $\lambda=0$. This can be seen if one realizes that the multicentered character of $U^{(\lambda)}(\mathbf{r})$, given in Eq. (41), leads to

$$U^{(\lambda)}_{\mathbf{k}}=u^{(\lambda)}_{\mathbf{k}}\sum_{j=1}^{N_p}\exp(i\mathbf{k}\cdot\mathbf{R}_j), \tag{50}$$

with $u^{(\lambda)}_{\mathbf{k}}$ the Fourier transform of $u^{(\lambda)}(\mathbf{r})$ defined in Eq. (42),

$$\begin{aligned}\beta u^{(\lambda)}_{\mathbf{k}}=&-4\pi lZ\frac{\exp(-\lambda R)}{k^2+\lambda^2}\\&\times\left[\gamma\cos(kR)+(1-\gamma)\frac{\sin(kR)}{kR}+(\lambda R)\frac{\sin(kR)}{kR}\right.\\&\left.+(\lambda R)^2(1-\gamma)\frac{\sin(kR)-kR\cos(kR)}{(kR)^3}\right].\end{aligned} \tag{51}$$

It is thus easily checked that for any wave vector $\mathbf{k}$,

$$\lim_{\lambda\to 0}(k^2+\lambda^2)\beta u^{(\lambda)}_{\mathbf{k}}=-4\pi lZ\left[\gamma\cos(kR)+(1-\gamma)\frac{\sin(kR)}{kR}\right]. \tag{52}$$

The inverse Fourier transformation of Eq. (48) leads, upon inserting Eqs. (50) and (52) in the limit $\lambda\to 0$, to the equilibrium profile $\rho(\mathbf{r})=\overline{\rho}+\Delta\rho(\mathbf{r})$ of the form

$$\rho(\mathbf{r})=\sum_{j=1}^{N_p}\rho_0(\mathbf{r}-\mathbf{R}_j), \tag{53}$$

with the spherically symmetric ''orbitals''

$$\begin{aligned}\rho_0(r)=&\frac{Z}{(2\pi)^3}\int d\mathbf{k}\exp(-i\mathbf{k}\cdot\mathbf{r})\frac{\kappa^2}{k^2+\kappa^2}\\&\times\left[\gamma\cos(kR)+(1-\gamma)\frac{\sin(kR)}{kR}\right]\\=&\begin{cases}\dfrac{Z_>\kappa^2}{4\pi}\dfrac{\exp(-\kappa r)}{r}, & r>R\\[2ex]\dfrac{Z_<\kappa^2}{4\pi}\dfrac{\sinh(\kappa r)}{r}, & r<R.\end{cases}\end{aligned} \tag{54}$$

The effective charges $Z_>$ and $Z_<$ are defined by

$$\begin{aligned}Z_>&=Z\left(\gamma\cosh(\kappa R)+(1-\gamma)\frac{\sinh(\kappa R)}{\kappa R}\right),\\Z_<&=Z\left(\frac{\exp(-\kappa R)}{\kappa R}\right)[1-\gamma(\kappa R+1)].\end{aligned} \tag{55}$$

For any γ,κ, and R, these profiles satisfy the normalization $\int d\mathbf{r}\rho_0(\mathbf{r})=Z$. To complete the specification of $\rho_0(\mathbf{r})$, a choice must be made for the yet undetermined parameter γ in the pseudopotential (27). According to Eqs. (54) and (55) the polyion-microion excluded volume condition is satisfied provided that

$$\gamma=\frac{1}{1+\kappa R}. \tag{56}$$

Substitution of Eq. (56) into Eq. (55) leads then directly to the DLVO value of the effective polyion valence [10],

$$Z_>=Z\left(\frac{\exp(\kappa R)}{1+\kappa R}\right). \tag{57}$$

The final expression for the microion-charge distribution, or double layer, around a polyion is thus

$$\rho_0(\mathbf{r})=\begin{cases}0, & r<R\\[2ex]\dfrac{Z\kappa^2}{4\pi}\dfrac{\exp(\kappa R)}{1+\kappa R}\dfrac{\exp(-\kappa r)}{r}, & r>R.\end{cases} \tag{58}$$

The coion and counterion density profiles $\rho_\pm(\mathbf{r})$ are obtained from Eq. (20) by taking the appropriate linear combination of $\sigma(\mathbf{r})$ and $\rho(\mathbf{r})$.

We finally note that even the choice for γ given in Eq. (56) and the resulting profile of Eqs. (53) and (58) do not take a truly proper account of the hard-core conditions. The reason is the same as encountered above for the equilibrium profiles of the hard-core functional $\mathcal{F}_{\rm hc}$: the profile around polyion i actually penetrates the core of any other polyion $j\neq i$. This shortcoming is, as already discussed, due to the linear relation between the inhomogeneity of the profile and the external potential of the polyions in the stationarity condition. Thus, although the key result summarized by Eqs. (53) and (58) is in itself not new (see, e.g., [9,10]), the present derivation shows that it is, in fact, the best charge-density profile within the framework of linearized Poisson-

Boltzmann theory (corresponding to the quadratic free-energy functional). Other choices of the pseudopotential parameter γ are possible. In particular, $\gamma=0$ leads back to the effective polyion valence $Z_>=Z\sinh(\kappa R)/\kappa R$ advocated by Sogami and Ise [23]. Clearly, however, this choice leads to microion orbitals that penetrate ''their own'' polyion cores, and is for that reason less favorable than the DLVO choice of Eq. (56).

IV. EFFECTIVE POLYION INTERACTION ENERGY

The microion-induced contribution F' to the effective polyion interaction energy is obtained by substituting the solutions $\sigma(\mathbf{r})$ and $\rho(\mathbf{r})$ of the Euler-Lagrange equations into the free-energy functional. This has already been achieved for the hard-core part, resulting in Eq. (38). As already stressed earlier, the explicit calculation of the minimum $F'_{\rm el}$ of $\mathcal{F}_{\rm el}$ is somewhat trickier, due to nontrivial cancellations between Coulomb divergences. This requires a detour via the auxiliary screened Coulomb potential (3), followed by the limit $\lambda\to 0$ once $F'_{\rm el}$ has been evaluated for any finite value of λ. The different steps of this procedure are detailed in Appendix A.

Gathering results from Eqs. (7), (21), (38), and (A11), we arrive at the final result for the potential energy in the effective one-component Hamiltonian,

$$V_p^{\rm eff}(\{\mathbf{R}_i\})=\Phi_0+\sum_{i<j}^{N_p} v_{\rm eff}(R_{ij}), \tag{59}$$

where $v_{\rm eff}(R)$ is the usual DLVO effective pair potential between polyions,

$$v_{\rm eff}(r)=\begin{cases}\infty, & r<2R\\ \dfrac{Z_>^2e^2}{\epsilon}\dfrac{\exp(-\kappa r)}{r}, & r>2R,\end{cases} \tag{60}$$

and where Φ_0 is a state-dependent term. This so-called volume term is *structure-independent*, i.e., it does not depend on the coordinates $\{\mathbf{R}_i\}$ of the polyions, and is given explicitly by

$$\begin{aligned}\Phi_0(V,T,n_p,n_s)=&F_{\rm id}(V,T,n_+)+F_{\rm id}(V,T,n_-)\\ &-\frac{Z^2e^2}{2\epsilon R}\frac{N_p\kappa R}{1+\kappa R}\\ &+k_BT\frac{\eta\bar{\sigma}}{1-\eta}V-\frac{1}{2}\frac{4\pi e^2}{\epsilon\kappa^2}(Zn_p)^2V,\end{aligned} \tag{61}$$

where $\bar{\sigma},\eta$, and κ are defined in Eqs. (25), (34), and (49). The last two terms on the right-hand side of Eq. (61) were erroneously omitted in our earlier analysis [19]. The importance of these terms, and more particularly of the latter, is well illustrated by the significant quantitative differences between the phase diagrams to be discussed later and those obtained in Ref. [19].

The existence of a volume term in the total polyion interaction energy is a consequence of the reduction (mapping) of the initial multicomponent system (polyions and microions) into an effective one-component system of ''dressed'' polyions. The third term on the right-hand side of Eq. (61) may be interpreted as the ''self-energy'' of the N_p electric double layers associated with the individual polyions, or as the energy due to the potential well in which the colloidal particles reside because of the surrounding oppositely charged distribution of microions. The fourth term accounts for additional excluded volume for the microions due to the hard core of the polyions; it vanishes for polyion radius $R=0$ since then $\eta=0$. It also vanishes in the salt-free case, i.e., when only polyions and counterions are left. The physical interpretation of the last terms of Eq. (61) is less transparent, however. It resembles, but is in general *not* identical to, the negative of the polyion-polyion mean-field contribution, $F_p^{\rm mf}$, to the total Helmholtz free energy, which with Eq. (60) can be evaluated as

$$\begin{aligned}F_p^{\rm mf}&=\frac{V}{2}n_p^2\int_{r>2R}d\mathbf{r}\,v_{\rm eff}(r)\\ &=\frac{1}{2}\frac{4\pi e^2}{\epsilon\kappa^2}(Zn_p)^2V\left(\frac{1+2\kappa R}{(1+\kappa R)^2}\right).\end{aligned} \tag{62}$$

The difference between $F_p^{\rm mf}$ and the last term of Eq. (61) is, apart from the minus sign, the bracketed factor in Eq. (62). This factor is unity only for point polyions, $R=0$. We therefore suggest that the final term of Eq. (61) is a reminder of the fact that the free energy of a purely Coulombic system is only due to correlations and fluctuations, and does not contain mean-field contributions because of the charge-neutrality condition. Since such a constraint does not hold for hard-core contributions, the cancellation of $F_p^{\rm mf}$ and the final term of Eq. (61) is not perfect for finite radius R of the polyion, due to the coupling of the Coulomb and hard-core contributions. Remarks along these lines have also been made by Warren in the appendix of Ref. [24].

In any given thermodynamic state, the volume term will have no influence on the equilibrium *structure* of the polyions which is entirely determined by the effective pair potential (60). Φ_0 does, however, contribute to all equilibrium *thermodynamic* properties of the system, including the polyion free energy, and is hence expected to have an influence on the phase diagram of the colloidal suspension. This will be examined in the next two sections.

V. FREE ENERGY OF THE COLLOIDAL SUSPENSION

Given the effective polyion interaction energy (59), the next task is to calculate the total free energy of the suspension, for fixed temperature T and volume V, as a function of the polyion and salt concentrations, or equivalently as a function of the colloid packing fraction η and the salt concentration n_s.

Substituting Eq. (59) into expression (4) for the total free energy we find that the latter naturally splits into three terms:

$$F=\Phi_0+F_p^{\rm (id)}+F_p^{\rm (exc)}, \tag{63}$$

where Φ_0 is given explicitly by Eq. (61), $F_p^{\rm (id)}$ is the trivial ideal free energy of a system of noninteracting polyions, and

$F_p^{(\mathrm{exc})}$ is the excess part of the free energy of polyions interacting via the effective pair potential (60),

$$F_p^{(\mathrm{exc})} = -k_B T \ln\left(\int \frac{d\mathbf{R}^{N_p}}{V^{N_p}} \exp\left(-\beta \sum_{i<j}^{N_p} v_{\mathrm{eff}}(R_{ij}) \right) \right). \tag{64}$$

This excess free energy may be calculated variationally, using the Gibbs-Bogoliubov inequality

$$F_p^{(\mathrm{exc})} \leqslant F_{\mathrm{ref}}^{(\mathrm{exc})} + \langle \Delta V \rangle_{\mathrm{ref}}, \tag{65}$$

where $F_{\mathrm{ref}}^{(\mathrm{exc})}$ is the excess free energy of a reference system under the same thermodynamic conditions but with pair potentials $v_{\mathrm{ref}}(R_{ij})$. The second term on the right-hand side of Eq. (65) is the ensemble average over the reference system, denoted $\langle \cdots \rangle_{\mathrm{ref}}$, of the potential-energy difference

$$\Delta V = \sum_{i<j}^{N_p} [v_{\mathrm{eff}}(R_{ij}) - v_{\mathrm{ref}}(R_{ij})]. \tag{66}$$

The right-hand side of Eq. (65) may be minimized with respect to one or several variational parameters characterizing the reference pair potential $v_{\mathrm{ref}}(r)$. This minimum, then, is the best estimate for the required quantity $F_p^{(\mathrm{exc})}$.

To calculate the variational free energy of the fluid phase, a hard-sphere (HS) reference system was adopted, and the right-hand side of Eq. (65) was minimized with respect to the reference hard-sphere diameter d, or equivalently the reference packing fraction $\eta_{\mathrm{ref}} = (\pi/6) n_p d^3$. The very accurate Carnahan-Starling equation of state was used for $F_{\mathrm{ref}}^{(\mathrm{exc})}$, while $\langle \Delta V \rangle_{\mathrm{ref}}$ was estimated using the Verlet-Weis improvement of the Percus-Yevick pair distribution function of the reference HS fluid [25]. The resulting upper bound estimates of the excess free energy of the Yukawa system, $f_Y^{(\mathrm{exc})} = \beta F_p^{(\mathrm{exc})}/N_p$, have been tested against ''exact'' Monte Carlo evaluations of this quantity. In these Monte Carlo simulations of $N_p = 256$ polyions we employ thermodynamic integration: for a given thermodynamic state point we gradually switch on the full pair interaction $v_{\mathrm{eff}}(r)$ starting from the hard-core fluid [26]. Typical results are reported in Fig. 1: the variational estimates are seen to lie very close to the ''exact'' results, as will be discussed in more detail below.

The excess free energy in the solid phase was calculated using an Einstein solid as a reference system. In this case the variational parameter is the single Einstein phonon frequency ω_E which determines all thermodynamic properties of the reference system, as well as the mean-square displacement of the particles around their lattice sites. The variational calculations were carried out for fcc and bcc lattices. Under all thermodynamic conditions which were explored, the free energy of the fcc lattice turned out to be slightly lower than that of the bcc crystal, but the differences are extremely small. The accuracy of the variational estimates was checked against MC calculations of the free energy based on the Frenkel-Ladd integration scheme [27], and against the predictions of a more realistic phonon model, described in Appendix B. The latter reproduce the MC data remarkably well, while the variational free energies turn out to be once more surprisingly accurate in view of the great simplicity of the calculation, as illustrated in Fig. 1.

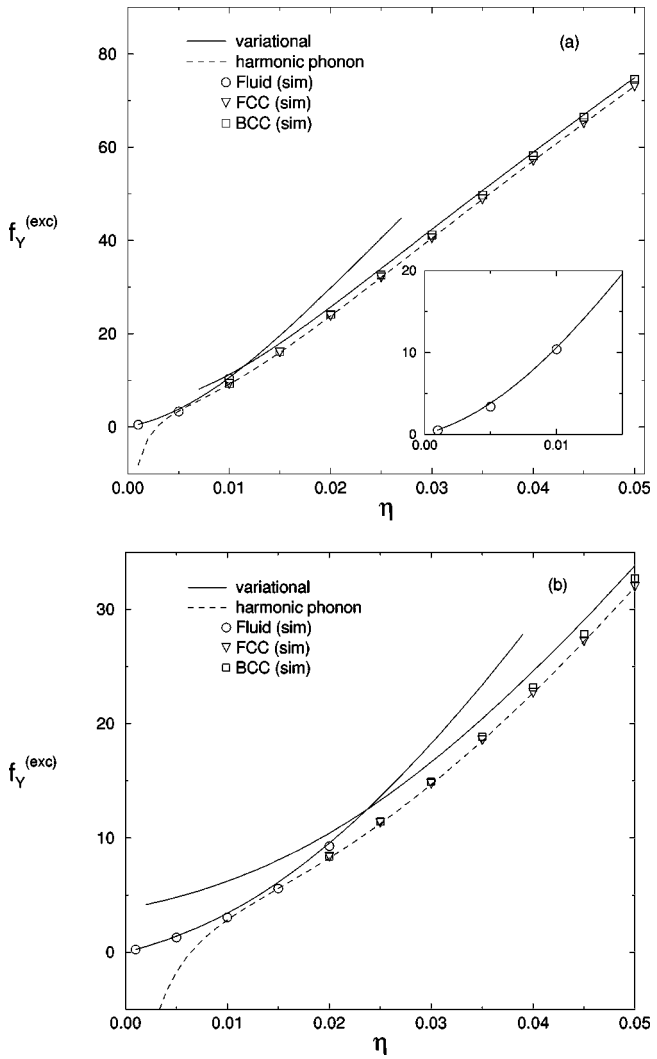

FIG. 1. Excess Helmholtz free energy $f_Y^{(\mathrm{exc})}$ (see text) of a one-component system with pairwise hard-core-Yukawa interactions (60) for charge $Z = 7300$ and diameter $D = 652$ nm, as a function of packing fraction η, for salt concentrations (a) $n_s = 1\ \mu M$ and (b) $n_s = 2\ \mu M$. The variational calculations (full curves) are in all cases above the results from ''exact'' Monte Carlo simulation. The harmonic phonon calculations for the solid free energy (dashed curve) reproduce the simulations perfectly, except at low densities, where its prediction of $f_Y^{(\mathrm{exc})}$ is pathologically low. The inset in (a) shows the fluid free energy in more detail.

As expected, the variational free energies (full curves) of both the fluid and the solid phase are slightly above their simulated values (symbols). The differences are small, however. The phonon model gives extremely accurate free energies in the solid phase, as follows from a comparison with the simulations in Fig. 1. Unfortunately, the model shows unphysical characteristics in the low-density regime, where it predicts pathologically low free energies for the solid phase. For that reason we merely used it as a test for the accuracy of the variational calculations, which prove to be reliable indeed. Consequently, the variational $F_p^{(\mathrm{exc})}$ was used throughout in the construction of the phase diagrams to be reported in the following section. We are thus in a position to com-

pute the total free energy (63) of the colloidal suspension systematically and efficiently for any set of thermodynamic conditions, as well as all relevant thermodynamic derivatives.

VI. PHASE DIAGRAMS

The phase diagram of a system of particles interacting via a screened Coulomb (Yukawa) potential of the form (60) (with $R=0$) is well known, thanks to the extensive simulation work of Robbins *et al.* [28]. As expected from the purely repulsive nature of the pair potential, the phase diagram exhibits a single high-temperature fluid phase, with a freezing line towards a low-temperature crystal phase, which is of fcc structure for large κ, and of bcc symmetry at small κ, with a bcc-fcc-fluid triple point around $\kappa n_p^{-1/3} \simeq 4.9$. These calculations do not take into account the state-dependence of the effective pair potential (60), embodied in the variations of κ and $Z_>$ with polyion and salt concentration. Neither do they include the state-dependent volume term (61). In this section we show that these factors have a profound influence on the topology of the phase diagram, particularly at low salt concentrations.

Due to the charge-neutrality constraints, the polyion-salt system behaves as a binary mixture characterized by three intensive variables, the temperature T, the polyion density n_p [or, equivalently, the packing fraction η as defined in Eq. (34)], and the salt (i.e., anion-cation pair) concentration n_s. To make contact with experimental conditions, all phase diagrams presented below were calculated at room temperature ($T=300$ K), and for a solvent dielectric constant $\epsilon=78$. This amounts to a Bjerrum length $l=e^2/\epsilon k_B T=7.2$ Å. For a given polyion diameter $D=2R$ and valence Z, the phase diagrams are represented in the (η, n_s) plane. At any given temperature T, the conditions of coexistence of two phases, labeled by 1 and 2, are the equalities of the chemical potentials of polyions (μ_p) and salt (μ_s), and of the osmotic pressures p,

$$\begin{aligned} \mu_p(n_p^{(1)}, n_s^{(1)}) &= \mu_p(n_p^{(2)}, n_s^{(2)}), \\ \mu_s(n_p^{(1)}, n_s^{(1)}) &= \mu_s(n_p^{(2)}, n_s^{(2)}), \\ p(n_p^{(1)}, n_s^{(1)}) &= p(n_p^{(2)}, n_s^{(2)}). \end{aligned} \tag{67}$$

The chemical potentials and pressures may be calculated from the free energy per unit volume, $\phi=F/V$, as obtained in the preceding section, by the usual thermodynamic relations

$$\begin{aligned} \mu_p &= \left(\frac{\partial \phi(n_p, n_s)}{\partial n_p} \right)_{n_s}, \\ \mu_s &= \left(\frac{\partial \phi(n_p, n_s)}{\partial n_s} \right)_{n_p}, \\ p &= n_p \mu_p + n_s \mu_s - \phi. \end{aligned} \tag{68}$$

In practice, phase coexistence is determined by fixing the salt concentration in one phase (e.g., $n_s^{(1)}$), and solving the set of three coupled equations (67) for the three remaining concentrations numerically. A practical problem of the numerical root-finding procedure involved is its poor convergence if the initial guess is far from the actual solution. The choice of a good initial guess is greatly facilitated by considering the Legendre transform to a ''semigrand potential'' $\omega=\phi-n_s\mu_s$, which describes the colloidal species canonically (fixed η) and the added salt grand-canonically (fixed μ_s). From curves $\omega(\eta, \mu_s)$ as a function of η at fixed μ_s, examples of which are shown in Fig. 2, common tangent constructions can be performed that are equivalent to solving Eqs. (68). We used a combination of these two numerical schemes to map out the full phase diagram in the (η, n_s) plane for various values of Z and D.

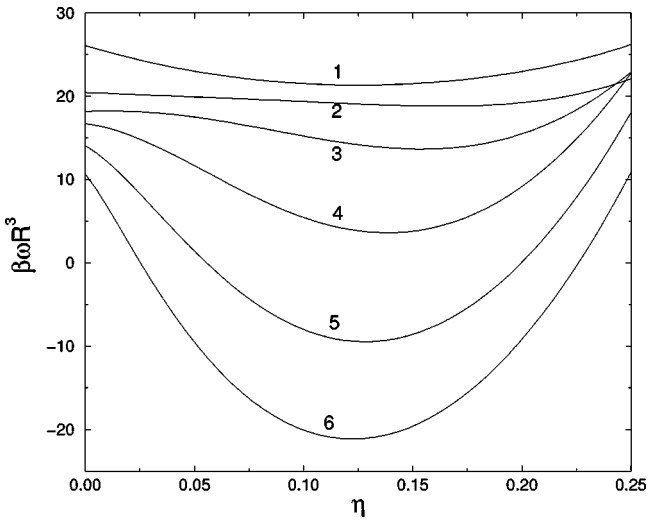

FIG. 2. Thermodynamic potential $\omega=\phi-\mu_s n_s$ in the fluid phase of colloids with charge $Z=3650$ and diameter $2R=462$ nm as a function of colloid packing fraction η at several fixed chemical potentials μ_s of the salt. The corresponding reservoirs are characterized by salt concentrations n_s^r of (1) 46.4 μM, (2) 21.5 μM, (3) 10.0 μM, (4) 4.64 μM, (5) 2.15 μM, and (6) 1.00 μM. The high-salt curve (1) is convex, and thus describes a stable homogeneous fluid phase; the lower salt curves exhibit concave parts from which common tangent constructions can be performed to yield the η's of the coexisting gas and liquid phases. Combination of such fluid curves with similar curves for the solid phase (not shown) can be used in the determination of fluid-solid coexistence.

In the strong screening (high salt-concentration) limit, such that $\kappa R \gg 1$, the two negative van der Waals–like contributions to the volume term (61) are nearly constant, or small, or linear in n_p, so that they are not expected to affect the phase diagram very much. This expectation is borne out by explicit calculations which show that for polyion diameters D of the order of a few hundred nanometers and valences Z of the order of a few thousand, the effect of the volume term Φ_0 is insignificant when $n_s \geqslant 20$ μM. For such sufficiently high n_s, our calculations predict a simple fluid-fcc solid phase coexistence similar to that observed when the volume term is omitted altogether [28]. The situation changes dramatically, however, at salt concentrations $n_s \leqslant 20$ μM, i.e., under highly deionized conditions typical of recent experimental data [8,11,12,14–16]. This is illustrated in Fig. 2, where the Legendre transform $\omega=\phi-n_s\mu_s$ discussed above is shown versus packing fraction at several

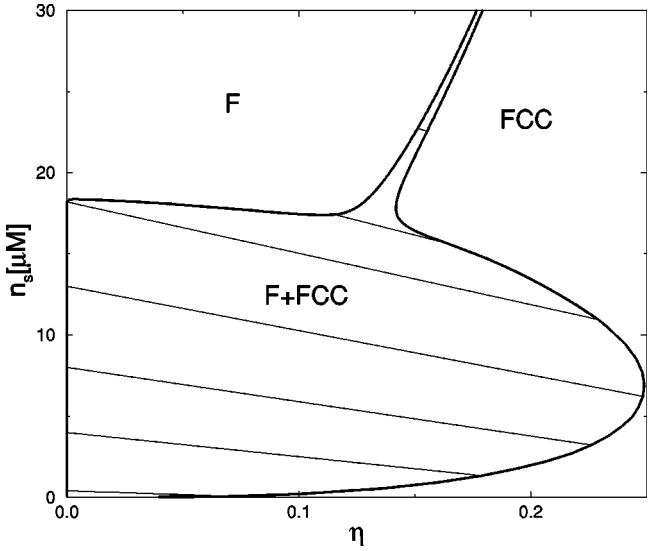

FIG. 3. Room-temperature phase diagram of aqueous colloidal suspension (charge $Z=7300$ and diameter $D=652$ nm) as a function of colloid packing fraction η and salt concentration n_s (μM). The narrow fluid (F) to fcc-solid transition at $n_s>20\ \mu M$ broadens and narrows again at lower salt concentrations. The (thinner) tie lines connect coexisting state points on the (thicker) phase boundaries.

fixed values of μ_s. These curves, which correspond to the fluid phase of a system with particle diameter $D=461$ nm and $Z=3650$, are seen to develop a concave region at sufficiently low reservoir salt concentration n_s^r (corresponding with μ_s), signaling a van der Waals–like instability which results in the separations into low- and high-density fluid phases of the colloidal particles.

Figures 3–6 show the evolution of the topology of the phase diagram with particle size and valence, assuming that $Z\sim R^2$ (i.e., the total polyion charge is proportional to the particle surface). The case of the largest particles ($Z=7300$ and $D=652$ nm) is plotted in Fig. 3. The fluid-solid phase

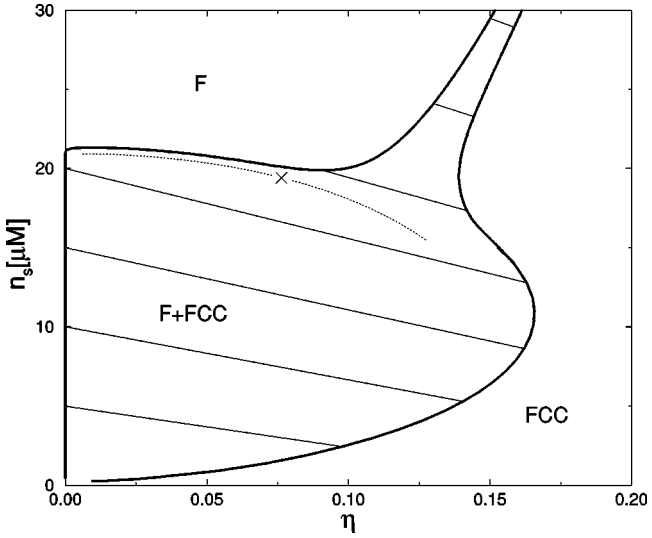

FIG. 4. As in Fig. 3, but with $Z=3650$ and $D=461$ nm. The dotted curve denotes a metastable gas-liquid binodal with the critical point indicated by $\times$.

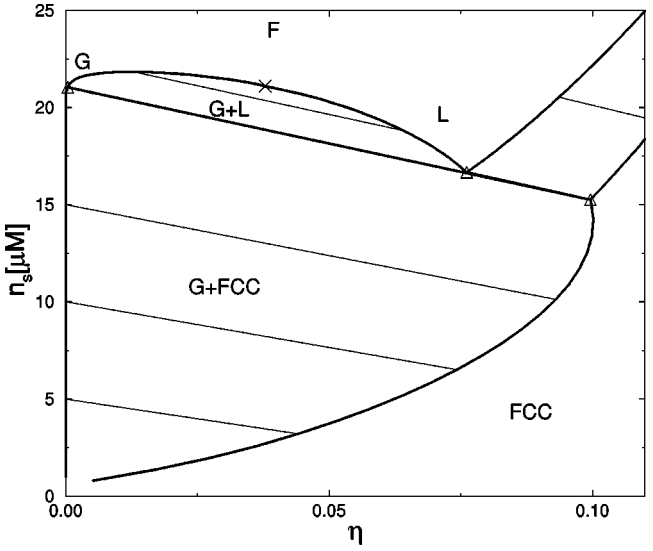

FIG. 5. As in Fig. 3, but with $Z=2086$ and $D=349$ nm. There is now stable coexistence of a gas (G) and liquid (L) phase between a critical point ($\times$) and triple points (Δ). Above the critical point the homogeneous fluid (F) phase is stable at low η and freezes into the fcc solid at higher η. Below the triple point, there is G-fcc coexistence.

transition, which for $n_s\geqslant 20\ \mu M$ is very ''narrow'' (i.e., shows only a small jump in colloid packing fraction), suddenly broadens enormously at lower n_s, signaling the coexistence of the fcc solid with a very low-density fluid. In fact, the fluid phase packing fraction is so low ($\eta<10^{-4}$) that the fluid side of the coexistence curve appears to coincide with the n_s axis on the scale of the figure. Note that as n_s is lowered below $20\ \mu M$, the packing fraction of the coexisting solid first increases, before decreasing at still lower salt concentrations (reentrant behavior). At the very lowest salt concentrations $n_s<1\ \mu M$, the dissociation of water becomes significant. Assuming a pH of 7, the concentrations of

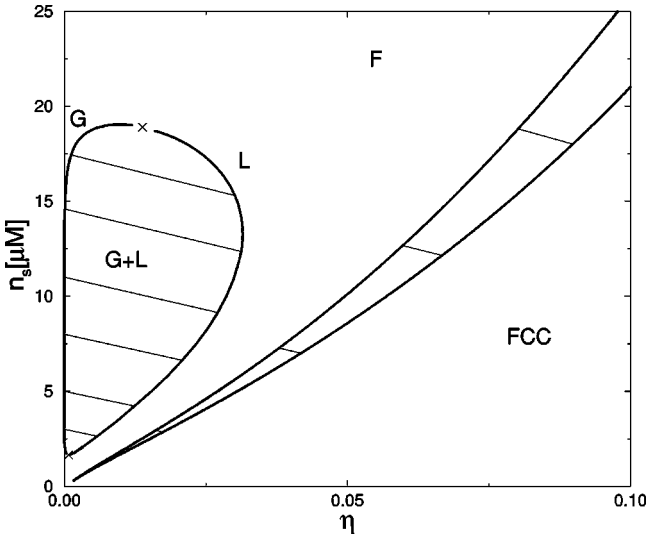

FIG. 6. As in Fig. 3, but with $Z=1217$ and $D=266$ nm. Here the van der Waals–like instability only persists at such low η that it is decoupled from the freezing transition. The G-L coexistence exhibits *two* critical points ($\times$) while the freezing transition does not show any broadening at low n_s.

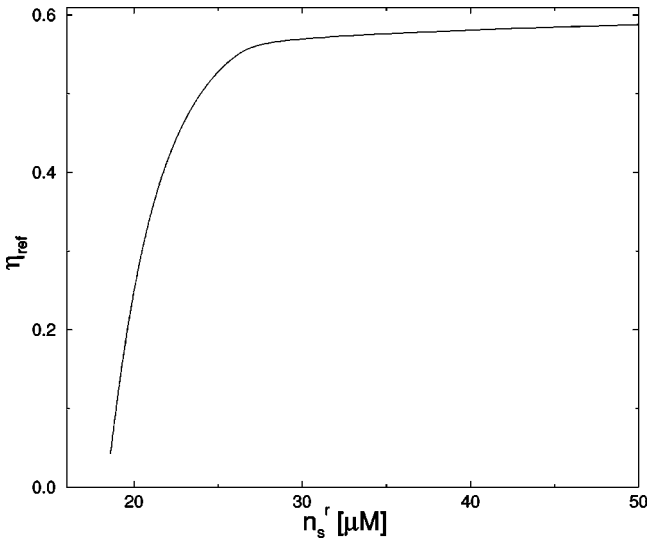

FIG. 7. The reference packing fraction η_{ref} (minimizing the Gibbs-Bogoliubov inequality) of the fluid phase that coexists with the fcc solid phase as a function of the reservoir salt concentration n_s^r for $Z=7300$ and $D=652$ nm. The sharp drop of η_{ref} below $n_s^r \approx 25\ \mu M$ indicates that the rule-of-thumb freezing criterion of $\eta_{\mathrm{eff}} \approx 0.5$ fails when the volume term Φ_0 affects freezing.

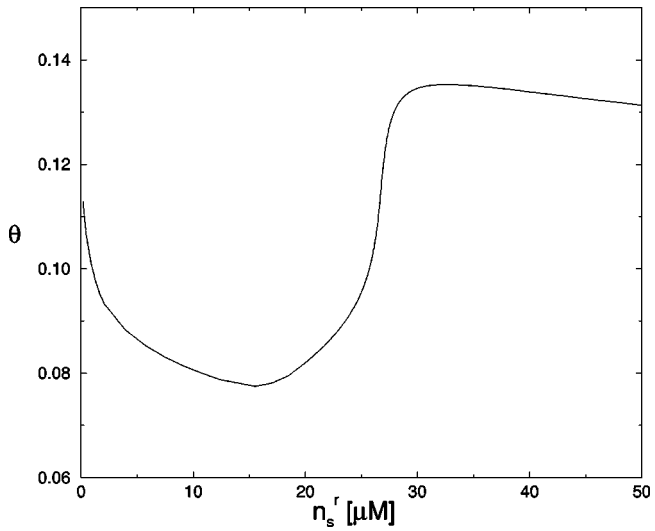

FIG. 8. Lindemann parameter θ of the fcc solid along the melting line as a function of the reservoir salt concentration n_s^r for the same system parameters as in Fig. 7. The melting criterion of $\theta \approx 0.15$ does hold at high n_s^r but fails below $n_s^r < 25\ \mu M$.

H^+ and OH^- ions have been added to the counterion and coion concentrations in all calculations; this does not have any significant effect as long as $n_s > 1\ \mu M$. The salt concentration in the coexisting phases may be read from the intersections of the inclined tie lines and the coexistence curves in Figs. 3–6.

The scenario changes continuously as Z decreases. In Fig. 4 ($Z=3650$, $D=461$ nm) the reentrant character on the solid side is less pronounced than for $Z=7300$, while a metastable fluid-fluid phase transition is barely preempted by the fluid-solid transition. For still lower charge (e.g., the case $Z=2086$ and $D=349$ nm is shown in Fig. 5) the fluid-fluid transition becomes stable with a ''gas-liquid'' critical point at a salt concentration n_s above that of a gas-liquid-solid triple point. This phase diagram roughly resembles that of a simple molecular system, where the temperature T plays the role of the salt concentration n_s in the colloidal dispersion. A difference is, of course, that the temperature in two coexisting phases is the same, while the salt concentrations need not necessarily be identical; the tie lines are therefore not horizontal in Figs. 3–6. At still lower charge the phase topology changes again, as illustrated in Fig. 6 for $Z=1217$ and $D=266$ nm. A reentrant ''gas-liquid'' coexistence curve, exhibiting an upper and a lower critical point, is now completely separated from the fluid-solid coexistence curve. Therefore there is no longer a triple point in this case. The fluid-solid-coexistence is now hardly affected by the volume term Φ_0 in the free energy. For particles and charges a few percent smaller than those of Fig. 6, the region of the fluid-fluid instability shrinks further and finally disappears completely, leading to a stable homogeneous fluid phase for packing fractions below the freezing line.

Figure 7 shows how the correspondence between the freezing transition in the colloidal suspension and that of an underlying HS transition is completely lost as soon as the contribution of the volume term becomes significant. The packing fraction η_{ref} of the HS reference fluid that minimizes the free energy of the fluid phase in the Gibbs-Bogoliubov inequality (65) is plotted as a function of n_s^r along the freezing line. Here n_s^r is the salt concentration in a reservoir at chemical potential μ_s. As long as n_s^r exceeds about $25\ \mu M$, η_{ref} is nearly constant, and reasonably close to the value ~ 0.5 corresponding to a hard-sphere fluid at freezing. Below that salt concentration, η_{ref} decreases sharply to a value near zero, indicative of a very dilute gas phase (a ''void''?) coexisting with the crystal.

The reentrant nature of the melting line is clearly illustrated in Fig. 8, which shows the variation of the Lindemann parameter θ in the coexisting solid with the reservoir salt concentration n_s^r. The Lindemann parameter is defined as the ratio of the root mean square of the displacement of a colloidal particle (from its equilibrium lattice position) and the lattice spacing (i.e., the nearest-neighbor distance). It is easily calculated from the Einstein solid that minimizes the free energy of the fcc colloidal crystal in the Gibbs-Bogoliubov inequality. While at the higher salt concentrations θ turns out to be fairly constant and close to the generally accepted ''universal'' value $\theta \approx 0.15$, it drops sharply at lower n_s^r, goes through a minimum, and then rises again at very low salt concentration. This behavior correlates well with the melting line of Fig. 3.

The Donnan effect is the reduction of salt concentration in a colloidal dispersion, compared to that of a reservoir at the same chemical potential μ_s, as the colloid packing fraction increases. This effect is illustrated in Fig. 9, which shows a family of n_s-η curves for 10 values of the chemical potential μ_s; the salt concentration in the reservoir corresponds to the n_s value at $\eta=0$. The figure shows that the Donnan effect becomes more pronounced as the reservoir concentration n_s^r decreases.

VII. DISCUSSION AND CONCLUSION

The present analysis shows that complex phase behavior may be expected in highly de-ionized charge-stabilized col-

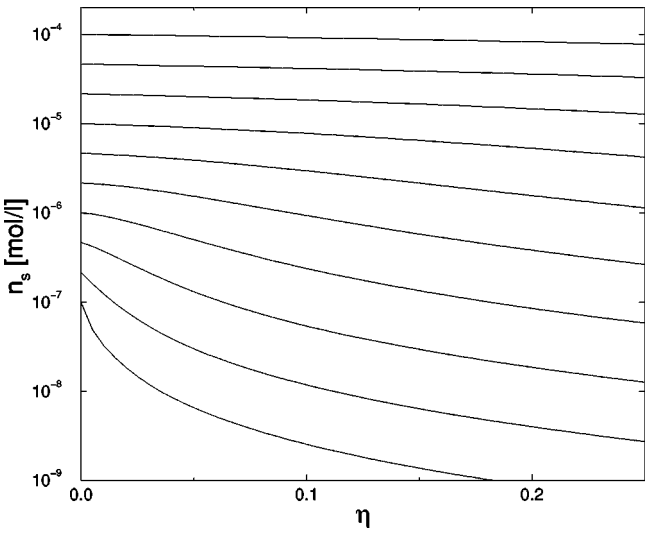

FIG. 9. Donnan effect for $Z=7300$ and $D=652$ nm. For each curve the salt chemical potential μ_s is fixed; the corresponding reservoir salt concentration n_s^r equals the value of n_s at $\eta=0$.

loidal dispersions. While long-range van der Waals attractions might induce fluid-fluid phase separation, and eventually irreversible flocculation, at high salt concentrations [20], the behavior predicted by the present analysis at very low salt concentrations is of purely electrostatic origin. The key finding is that charge-stabilized colloidal particles may undergo a fluid-fluid (or gas-liquid) phase separation for sufficiently low ionic strengths, although they interact via a purely repulsive effective pair potential. In other words, the experimental observations of a fluid-fluid phase transition do not necessarily imply the existence of attractive forces between the charged colloidal particles or polyions. This seemingly surprising result is a direct consequence of the reduction of the initial multicomponent problem, involving mesoscopic polyions and microscopic coions and counterions, to a one-component system of dressed polyions interacting via effective screened forces; the effective interactions are pairwise additive only within the framework of the approximate, quadratic functional introduced in Sec. III. The price to pay for this reduction is the appearance of the state-dependent volume term Φ_0 in the free energy, which has a profound effect on the phase behavior of the colloidal dispersion. The reduction also leads to a decoupling between density fluctuations, characterized by the measurable polyion structure factor $S(k)$, and the observed thermodynamic behavior. In a genuine one-component system, fluid-fluid phase separation is signaled by enhanced density fluctuations near the critical point, resulting in a sharp increase of the structure factor at small k (long wavelengths). In the effective one-component system of dressed colloidal particles, $S(k)$ is unaffected by the vicinity of the critical point of the fluid-fluid phase transition, since it is determined by the purely repulsive effective pair potential (60), which can only lead to regular behavior in the $k\rightarrow 0$ limit.

It is worth noting that a volume term similar to Φ_0 also occurs naturally in the theory of simple metals, where the full ion-electron system is mapped onto a system of pseudoatoms interacting via an effective state-dependent pair potential [21]. However, in the metal case this volume term does not have a significant incidence on phase behavior because of the restricted range of electron densities and ionic charges. In the colloid case the parameter space is much wider due to the large range of variation of n_p, R, and Z, and due to the existence of an additional salt component, which has no analog in metals.

The wealth of possible phase diagrams, induced by the structure-independent contribution Φ_0 to the free energy, is illustrated in Figs. 3–6, which summarize the most remarkable scenarios. For large, highly charged polyions, the fluid-fcc solid freezing transition dramatically widens below a salt concentration of about 20 μM; the packing fraction of the coexisting fluid drops to extremely small values while that of the coexisting fcc crystalline phase exhibits a reentrant feature upon lowering n_s. The sudden broadening of the fluid-solid density gap is attributed to an underlying metastable fluid-fluid phase separation. This is shown explicitly by the results for smaller polyions in Figs. 4 and 5: the initially metastable fluid-fluid transition (Fig. 4) becomes stable as the polyion size and charge decreases, with the emergence of a fluid-fluid critical point above a fluid-fluid-solid triple point. This scenario is vaguely reminiscent of the phase diagrams observed in sterically stabilized colloidal suspensions in the presence of free polymer coils [4,6]. However, in this case the change in topology of the phase diagram is induced by a change in the range of the effective depletion interaction, which is essentially attractive, while a volume term similar to Φ_0 has no incidence on the phase diagram. Finally, for yet smaller polyions (Fig. 6), the triple point disappears, and the fluid-fluid part of the phase diagram completely separates from the fluid-solid coexistence line, with the appearance of a lower fluid-fluid critical point. Note that in both Figs. 5 and 6 the packing fractions of the low-density ''gas'' phase are always very small [except very close to the critical point(s)], which may provide an explanation for the observed ''voids'' reported in Ref. [15]. For diameters and charges a few percent smaller than those of Fig. 6, the fluid-fluid instability shrinks to a smaller η-n_s region, and finally disappears completely.

The possibility of a fluid-fluid phase separation of suspensions or solutions of like-charged polyions was already suggested by Langmuir [29], who referred to it as ''unipolar coarcervation.'' His argument was only qualitative, and based on the behavior of the osmotic pressure, evaluated within Debye-Hückel theory for simple electrolytes. A similar, more careful argument was put forward in the thesis of Voorn [30], with specific applications to linear polyelectrolytes. He pointed out that the addition of salt decreases the tendency for phase separation, in qualitative agreement with the predictions of the present work. However, neither Langmuir's nor Voorn's considerations are directly applicable to the case of highly charged colloidal particles considered here. More recent studies of effective interactions between charged colloidal particles in suspension have revealed interesting mechanisms for pairwise attraction. Some of these require multivalent salt ions, and originate from correlations and fluctuations in the double layers [31,32]. The resulting attractions are, however, very short-ranged, and can therefore probably not drive a fluid-fluid transition. Moreover, it was shown in Ref. [33] that a spherical geometry of the particles suppresses attractions compared to a plate geometry. In Ref.

[34] another mechanism for attraction is put forward. The attraction there originates from the Coulomb-depletion effect caused by an intricate interplay between Coulombic and steric interactions. It would be interesting to study its effect, together with the volume term introduced here, on the phase diagrams.

The main conclusion of this paper, namely the possibility of a fluid-fluid phase separation due to Coulombic and excluded volume interactions alone, is reminiscent of a similar phase separation predicted for very dilute symmetric electrolytes, modeled by the ''restricted primitive model'' [35] of oppositely charged hard spheres. Both in this symmetric model and in the extremely asymmetric case investigated here, the phase separation is driven by a delicate balance between like-charge repulsion and opposite-charge attraction. The polyion-microion asymmetry and the presence of salt appear, however, to add further complexity to the phase diagrams.

ACKNOWLEDGMENTS

The authors have benefited from discussions with J.Th.G. Overbeek, H.N.W. Lekkerkerker, T. Biben, A. van Blaaderen, and, particularly, P.B. Warren and R. Evans. They are grateful to A. Vrij and H.N.W. Lekkerkerker for pointing out the work by Voorn [30], and to the ''Ecole Normale Supérieure de Lyon'' and CECAM for hospitality during the initial stages of this work. R.v.R. also thanks P.B. Warren for sending notes on the subtleties involved in the divergent Coulomb integrals. This work was supported by Grant Nos. ERBFMBICT971869 and ERBFMBICT972446 of the TMR Program, by EPSRC Grant No. GR/L89013, and by the EPSRC Liquid Matter Network.

APPENDIX A

In this appendix we calculate the minimum value $F'_{\rm el}$ of the functional $\mathcal{F}_{\rm el}$ defined in Eq. (22) by inserting the minimizing profile (53). It proves essential to use the regularized Coulomb potential (3) throughout, and take the limit $\lambda\to 0$ at late stages of the calculation. It proves convenient to use the Fourier representation throughout. In this representation the functional reads

$$\beta\mathcal{F}_{\rm el}=\frac{1}{2n}\frac{1}{(2\pi)^3}\int d\mathbf{k}\frac{k^2+\kappa_\lambda^2}{k^2+\lambda^2}\Delta\rho^{(1)}_{-\mathbf{k}}\Delta\rho^{(1)}_{\mathbf{k}} + \frac{1}{(2\pi)^3}\int d\mathbf{k}\beta U^{(\lambda)}_{-\mathbf{k}}\Delta\rho^{(1)}_{\mathbf{k}}+\overline{\rho}\beta U^{(\lambda)}_{\mathbf{k}=\mathbf{0}}+\frac{1}{2}\frac{4\pi l}{\lambda^2}\overline{\rho}^2V, \tag{A1}$$

with $U^{(\lambda)}_{\mathbf{k}}$ defined in Eqs. (50) and (51), κ and κ_λ in Eq. (49), $n=n_++n_-$ the total microion number density, and $l=e^2/\epsilon k_BT$ the Bjerrum length. Inserting the equilibrium profile of Eq. (48) into the functional (A1) gives its minimum value

$$\beta F'_{\rm el}=-\frac{n}{2}\frac{1}{(2\pi)^3}\int d\mathbf{k}\frac{k^2+\lambda^2}{k^2+\kappa_\lambda^2}\beta U^{(\lambda)}_{-\mathbf{k}}\beta U^{(\lambda)}_{\mathbf{k}} +\frac{n}{2V}\frac{\lambda^2}{\kappa_\lambda^2}(\beta U^{(\lambda)}_{\mathbf{k}=\mathbf{0}})^2+\overline{\rho}\beta U^{(\lambda)}_{\mathbf{k}=\mathbf{0}}+\frac{1}{2}\frac{4\pi l}{\lambda^2}\overline{\rho}^2V. \tag{A2}$$

We first focus on the evaluation of the second line of (A2), and then treat the first line.

It follows directly from Eq. (50) that $U^{(\lambda)}_{\mathbf{k}=\mathbf{0}}=N_pu^{(\lambda)}_{\mathbf{k}=\mathbf{0}}$, and hence from Eq. (51) that

$$\overline{\rho}\beta U^{(\lambda)}_{\mathbf{k}=\mathbf{0}}=-4\pi l\overline{\rho}Zn_p\left(\frac{1}{\lambda^2}-\frac{R^2(1+2\gamma)}{6}\right)V+\mathcal{O}(\lambda R), \tag{A3}$$

where the $\mathcal{O}(\lambda R)$ are irrelevant in the limit of interest $\lambda\to 0$. A similar expansion reveals

$$\frac{n}{2V}\frac{\lambda^2}{\kappa_\lambda^2}(\beta U^{(\lambda)}_{\mathbf{k}=\mathbf{0}})^2=4\pi l(Zn_p)^2\left(\frac{1}{2\lambda^2}+\frac{R^2(1+2\gamma)}{6}-\frac{1}{\kappa^2}\right)V +\mathcal{O}(\lambda R,\lambda^2/\kappa^2). \tag{A4}$$

Using the results of Eqs. (A3) and (A4) in the evaluation of the second line of Eq. (A2) yields, neglecting the $\mathcal{O}(\lambda R,\lambda^2/\kappa^2)$ terms,

$$\begin{aligned}\frac{n}{2V}\frac{\lambda^2}{\kappa_\lambda^2}(\beta U^{(\lambda)}_{\mathbf{k}=\mathbf{0}})^2+\overline{\rho}U^{(\lambda)}_{\mathbf{k}=0}+\frac{1}{2}\frac{4\pi l}{\lambda^2}\overline{\rho}^2V&=\frac{1}{2}\frac{4\pi l}{\lambda^2}(Zn_p-\overline{\rho})^2V-\frac{1}{2}\frac{4\pi l}{\kappa^2}(Zn_p)^2V\\&=-\frac{1}{2}\frac{4\pi l}{\kappa^2}(Zn_p)^2V,\end{aligned} \tag{A5}$$

where we used the electroneutrality condition $\overline{\rho}=Zn_p$. The γ-dependent contributions cancel identically. The remaining term of Eq. (A5) is independent of λ, and therefore constitutes the $\lambda\to 0$ limit of the second line of Eq. (A2).

We now calculate the first line of Eq. (A2), which can be rewritten with Eq. (50) as

$$\begin{aligned}-\frac{n}{2}\frac{1}{(2\pi)^3}\int d\mathbf{k}\frac{k^2+\lambda^2}{k^2+\kappa_\lambda^2}\beta u^{(\lambda)}_{-\mathbf{k}}\beta u^{(\lambda)}_{\mathbf{k}}\sum_{i=1}^{N_p}\sum_{j=1}^{N_p}\exp(i\mathbf{k}\cdot\mathbf{R}_{ij})&=-\frac{n}{2}\frac{4\pi}{(2\pi)^3}\sum_{i=1}^{N_p}\sum_{j=1}^{N_p}\int_0^\infty dk\frac{\sin(kR_{ij})}{kR_{ij}}\\&\times\frac{k^2(k^2+\lambda^2)}{k^2+\kappa_\lambda^2}\beta u^{(\lambda)}_{-\mathbf{k}}\beta u^{(\lambda)}_{\mathbf{k}},\end{aligned} \tag{A6}$$

where we performed the angular integrals explicitly. It follows from Eq. (51) and a straightforward λ expansion that

$$\frac{k^2(k^2+\lambda^2)}{k^2+\kappa_\lambda^2}\beta u_{-\mathbf{k}}^{(\lambda)}\beta u_{\mathbf{k}}^{(\lambda)} = \frac{(4\pi lZ)^2}{k^2+\kappa^2}\left(\gamma\cos(kR)+(1-\gamma)\frac{\sin(kR)}{kR}\right)^2 + \mathcal{O}(\lambda R,\lambda^2/\kappa^2), \tag{A7}$$

which upon insertion into Eq. (A6) leads to integrals that can be performed easily with contour integration techniques. The terms in the double sum in Eq. (A6) must then be distinguished between those with $i=j$ (for which $R_{ij}=0$) and those with $i\neq j$ (for which $R_{ij}>2R$ because of the hard-core repulsion between the polyions). The terms $i\neq j$ give rise to the integral

$$\begin{aligned}-\frac{n}{4}\frac{4\pi}{(2\pi)^3}\int_{-\infty}^{\infty}dk\frac{\sin(kR_{ij})}{kR_{ij}} &\times\frac{(4\pi lZ)^2}{k^2+\kappa^2}\left(\gamma\cos(kR)+(1-\gamma)\frac{\sin(kR)}{kR}\right)^2\\ &=\frac{Z^2l}{2}\left(\gamma\cosh(\kappa R)+(1-\gamma)\frac{\sinh(\kappa R)}{\kappa R}\right)^2\\ &\times\frac{\exp(-\kappa R_{ij})}{R_{ij}}-\frac{Z^2l}{2}\frac{1}{R_{ij}}\\ &=\frac{Z_>^2l}{2}\frac{\exp(-\kappa R_{ij})}{R_{ij}}-\frac{Z^2l}{2}\frac{1}{R_{ij}},\end{aligned} \tag{A8}$$

where we used the definition of the effective charge $Z_>$ of Eq. (55). The factors 1/2 in Eq. (A8) correct for double counting of $i\neq j$ terms in the double sum in Eq. (A6). The terms $i=j$ in Eq. (A6) give rise to N_p identical integrals

$$-\frac{n}{4}\frac{4\pi}{(2\pi)^3}\int_{-\infty}^{\infty}dk\frac{(4\pi lZ)^2}{k^2+\kappa^2}\left(\gamma\cos(kR)+(1-\gamma)\frac{\sin(kR)}{kR}\right)^2 = -\frac{Z^2l}{2}\kappa h(\gamma,\kappa R), \tag{A9}$$

where the dimensionless function $h(\gamma,x)$ is given by

$$h(\gamma,x)=(1-\gamma)^2\frac{\exp(-2x)-1+2x}{2x^2} + 2\gamma(1-\gamma)\frac{1-\exp(-2x)}{2x}+\gamma^2\frac{\exp(-2x)+1}{2}. \tag{A10}$$

Gathering the results of this appendix reduces $F'_{\rm el}$ from Eq. (A2) to

$$F'_{\rm el}=\sum_{i<j}^{N_p}\left(\frac{Z_>^2e^2}{\epsilon}\frac{\exp(-\kappa R_{ij})}{R_{ij}}-\frac{Z^2e^2}{\epsilon}\frac{1}{R_{ij}}\right) - \frac{1}{2}\frac{4\pi e^2}{\epsilon\kappa^2}(Zn_p)^2V-\frac{Z^2e^2}{2\epsilon}\kappa h(\gamma,\kappa R)N_p. \tag{A11}$$

The first line in Eq. (A8) is recognized as the difference between screened and bare Coulomb interactions of all pairs of polyions at separations R_{ij}, with the effective charge number $Z_>$ determining the strength of the pairwise screened repulsions. The bare Coulomb interactions cancel, in the calculation of the effective polyion potential $V_p^{(\rm eff)}$, the bare polyion-polyion contribution from H_p of Eq. (3). The second line of Eq. (A11) is independent of the coordinates $\mathbf{R}_i$ of the polyions. Its first term, which was missed in the analysis of Ref. [19], appears after carefully taking the limit $\lambda\to 0$. Its physical interpretation is discussed in the main text.

It is easily checked that $h((1+x)^{-1},x)=(1+x)^{-1}$, and hence the second term in the second line of Eq. (A11) equals, for each of the N_p polyions, $-(Ze)^2/[2\epsilon(\kappa^{-1}+R)]$ for our choice $\gamma=(1+\kappa R)^{-1}$. This is of the order of the Coulombic energy of charges $-Ze$ and $+Ze$ separated by a distance $\kappa^{-1}+R$ in a medium of dielectric constant ϵ. It thus represents the self-energy of an N_p dressed polyion, i.e., bare polyions of charge $-Ze$ with double layers of thickness κ^{-1} and net charge $+Ze$. It can also be interpreted as the potential energy of the N_p polyions due to the potential well created by the double layers. For the Sogami-Ise choice $\gamma=0$, it is easily checked from $h(0,x)=[\exp(-2x)-1+2x]/(2x^2)$ that the second term in the second line of Eq. (A11) gives rise to a free-energy contribution $(Ze)^2/(4\epsilon R)[\exp(-\kappa R)-1+2\kappa R]/(\kappa R)$ per colloidal particle. This contribution is identical to the one in Eq. (44) of Ref. [23]. Although it has the same characteristics as the one we obtained from $\gamma=1/(1+\kappa R)$, it was not considered as a driving term for phase separation in Ref. [23]. Instead, the focus there has been on the (controversial) transformation from the Helmholtz to Gibbs effective pair interaction [36].

APPENDIX B

We calculate the free energy F_D of a system of $N=nV$ independent three-dimensional harmonic oscillators of mass m fixed on N sites in a volume V. Throughout we assume a Debye spectrum

$$\omega_s(\mathbf{k})=c_s|\mathbf{k}| \tag{B1}$$

for the longitudinal ($s=1$) and transversal ($s=2,3$) modes. Later on we adjust the sound velocities $c_s(s=1,2,3)$ to be consistent with the screened Coulomb pair potentials given in Eq. (60), such that $F_D+\Phi_0$ is an estimate for the free energy F of the solid phase of a colloidal crystal. Within classical statistical mechanics, each mode contributes an amount $k_BT\ln[\hbar\omega_s(\mathbf{k})/k_BT]$ to the total free energy F_D, while the ground-state energy, or Madelung energy, contributes an amount u_m per particle. Hence we have formally

$$F_D = Nu_m + k_BTV\int d\omega g(\omega)\ln[\hbar\omega/k_BT], \qquad \text{(B2)}$$

where we introduced the total phonon density $g(\omega) = \Sigma_{s=1}^{3} g_s(\omega)$. The phonon density $g_s(\omega)$ of the branches $s = 1,2,3$ is defined by

$$g_s(\omega) \equiv \frac{1}{(2\pi)^3}\int d\mathbf{k}\,\delta[\omega - \omega_s(\mathbf{k})] = \begin{cases} \omega^2/(2\pi^2 c_s^3), & \omega \leqslant \omega_{s,D} \\ 0, & \omega > \omega_{s,D}, \end{cases} \qquad \text{(B3)}$$

where we used Eq. (B1) and introduced the Debye frequency $\omega_{s,D} \equiv c_s k_D$. The Debye wave number k_D is a cutoff such that the normalization condition $\int_0^\infty d\omega g(\omega) = 3n$ is satisfied, i.e., $k_D = (6\pi^2 n)^{1/3}$. Inserting Eq. (B3) into Eq. (B2) and performing the elementary integrals yields

$$\frac{F_D}{Nk_BT} = u_m/k_BT + \ln(n\Lambda^3) - 1 + \ln[3\sqrt{\pi/2}] + \frac{1}{2}\sum_{s=1}^{3}\ln[mc_s^2/k_BT], \qquad \text{(B4)}$$

with thermal wavelength $\Lambda = \hbar/\sqrt{2\pi m k_B T}$. The first line of Eq. (B4) is the Madelung and ideal gas contribution, the second line is the excess part in terms of the sound velocities c_s, to be calculated below.

We now introduce the even moments μ_{2j} of the phonon distribution,

$$\mu_{2j} = \int d\omega g(\omega)\omega^{2j} \quad (j = 1,2,3,\ldots). \qquad \text{(B5)}$$

It is easily checked from Eq. (B3) that the Debye spectrum gives rise to

$$\frac{m\mu_2}{k_BT} = \frac{3nk_D^2}{5}\sum_{s=1}^{3}\frac{mc_s^2}{k_BT}, \qquad \frac{m^2\mu_4}{(k_BT)^2} = \frac{3k_D^4 n}{7}\sum_{s=1}^{3}\left(\frac{mc_s^2}{k_BT}\right)^2. \qquad \text{(B6)}$$

If we realize that $c_1 \equiv c_\parallel$ and $c_2 = c_3 \equiv c_\perp$, then Eq. (B6) constitutes two equations for the two unknown longitudinal ($c_\parallel$) and transversal ($c_\perp$) sound velocities, in terms of the yet unknown moments μ_2 and μ_4. We now calculate these moments independently in terms of the pair potential $v(\mathbf{r})$ between the particles that constitute the harmonic solid; the sound velocities $c_\parallel$ and $c_\perp$ can then uniquely be determined from Eq. (B6), and the free energy from Eq. (B4).

First we use that the spectrum (B1) is actually defined such that $m\omega_s^2(\mathbf{k})$ for $s = 1,2,3$ are the eigenvalues of the 3×3 dynamical matrix

$$D_{\mathbf{k}} = \sum_{\mathbf{R}} D(\mathbf{R})\exp(i\mathbf{k}\cdot\mathbf{R}), \qquad \text{(B7)}$$

where the sum is over a Bravais lattice, and where

$$D(\mathbf{R}-\mathbf{R}') = -(\boldsymbol{\nabla}\boldsymbol{\nabla}v)(\mathbf{R}-\mathbf{R}') + \delta_{\mathbf{R},\mathbf{R}'}\sum_{\mathbf{R}''}(\boldsymbol{\nabla}\boldsymbol{\nabla}v)(\mathbf{R}-\mathbf{R}'') \qquad \text{(B8)}$$

is a 3×3 matrix involving tensor combinations of the gradient operator $\boldsymbol{\nabla}$. Since $m\omega_s(\mathbf{k})^2$ for $s = 1,2,3$ are eigenvalues of $D_{\mathbf{k}}$, it follows that for any $j = 1,2,\ldots,$

$$\mathrm{Tr}\,(D_{\mathbf{k}})^j = \sum_{s=1}^{3}(m\omega_s^2(\mathbf{k}))^j, \qquad \text{(B9)}$$

where Tr is the trace over a 3×3 matrix. Hence we have for the even moments

$$\mu_{2j} = \frac{1}{(2\pi)^3}\int_{k<k_D} d\mathbf{k}\sum_{s=1}^{3}\omega_s^{2j}(\mathbf{k}) = \frac{n}{m^j}\mathrm{Tr}\left(\sum_{\mathbf{R}} D(\mathbf{R})\frac{3\sin(k_DR) - 3k_DR\cos(k_DR)}{(k_DR)^3}\right)^j \approx \frac{n}{m^j}\mathrm{Tr}(D(\mathbf{R}=0))^j, \qquad \text{(B10)}$$

where we used $n = k_D^3/6\pi^2$ and the oscillating character and rapid decay of the fraction between the large parentheses in the second line. We are interested in a spherically symmetric potential $v(r)$, with radial derivatives $v'(r) = dv(r)/dr$ and $v''(r) = d^2v(r)/dr^2$, and hence

$$\boldsymbol{\nabla}v(\mathbf{r}) = v'(r)\hat{\boldsymbol{r}}, \qquad \boldsymbol{\nabla}\boldsymbol{\nabla}v(\mathbf{r}) = \frac{v'(r)}{r}\mathbf{I} + \left(v''(r) - \frac{v'(r)}{r}\right)\hat{\boldsymbol{r}}\hat{\boldsymbol{r}}, \qquad \text{(B11)}$$

with the 3×3 unit matrix $\mathbf{I}$ and radial unit vector $\hat{\boldsymbol{r}} = \mathbf{r}/r$. Using that $\mathrm{Tr}\,\mathbf{I} = 3$, $\mathrm{Tr}\,\hat{\boldsymbol{r}}\hat{\boldsymbol{r}}' = \hat{\boldsymbol{r}}\cdot\hat{\boldsymbol{r}}'$, and $\mathrm{Tr}\,\boldsymbol{\nabla}\boldsymbol{\nabla} = \Delta$, the Laplacian, we can write from Eqs. (B8) and (B10) that

$$\frac{m\mu_2}{k_BT} = \frac{n}{k_BT}\sum_{\mathbf{R}\neq\mathbf{0}}\Delta v(R),$$

$$\frac{m^2\mu_4}{(k_BT)^2} = \frac{n}{(k_BT)^2}\left(\sum_{\mathbf{R}\neq 0}\{[v''(R)]^2 + 2[v'(R)/R]^2\}\right) + \frac{n}{(k_BT)^2}\mathrm{Tr}\left(\sum_{\mathbf{R}\neq\mathbf{0}}(\boldsymbol{\nabla}\boldsymbol{\nabla}v)(\mathbf{R})\right)^2. \qquad \text{(B12)}$$

The numerical evaluation of the final term in Eq. (B12) is greatly facilitated by the fact that the matrix

$$M \equiv \sum_{\mathbf{R}\neq\mathbf{0}}(\boldsymbol{\nabla}\boldsymbol{\nabla}v)(R) \qquad \text{(B13)}$$

is diagonal in the basis of the principal crystallographic directions $\hat{\boldsymbol{x}},\hat{\boldsymbol{y}},\hat{\boldsymbol{z}}$ due to the inversion symmetry of the lattice. Moreover, due to isotropy all three eigenvalues are identical and hence from Eq. (B11) we have

$$M = \mathbf{I} \sum_{\mathbf{R} \neq \mathbf{0}} \left[\frac{v'(R)}{R} + \left(v''(R) - \frac{v'(R)}{R} \right) (\hat{\mathbf{R}} \cdot \hat{\mathbf{z}})^2 \right]. \quad \text{(B14)}$$

Using Eq. (B14) it is straightforward to evaluate the lattice sums in Eq. (B12) for a given pair potential $v(r)$; the lattice constant a (along a principal axis) is fixed by the number density and the symmetry of the lattice. For fcc we have $a = (4/n)^{1/3}$, for bcc $a = (2/n)^{1/3}$. The resulting numerical values for μ_2 and μ_4 then provide the left-hand side of Eq. (B6) explicitly, from which numerical values for the dimensionless sound velocities $mc_{\parallel}^2/k_BT$ and $mc_{\perp}^2/k_BT$ follow. These can, subsequently, be used to evaluate the second line of Eq. (B4). The full evaluation of F_D also requires the Madelung energy u_M, given by the lattice sum

$$u_m = \sum_{\mathbf{R} \neq \mathbf{0}} v(R), \quad \text{(B15)}$$

which can also be evaluated directly numerically for a given $v(r)$.

[1] J.S. Rowlinson and F. Swinton, *Liquids and Liquid Mixtures*, 3rd ed. (Butterworths, London, 1982).

[2] S. Asakura and F. Oosawa, J. Polym. Sci. **33**, 183 (1958); A. Vrij, Pure Appl. Chem. **48**, 471 (1976).

[3] The depletion force has been reassessed in a number of recent papers: see, e.g., Y. Mao, M.E. Cates, and H.N.W. Lekkerkerker, Physica A **222**, 10 (1995); T. Biben, P. Bladon, and D. Frenkel, J. Phys.: Condens. Matter **8**, 10 799 (1996); R. Dickman, P. Attard, and V. Simonian, J. Chem. Phys. **107**, 205 (1997); B. Götzelmann, R. Evans, and S. Dietrich, Phys. Rev. E **57**, 6785 (1998).

[4] A.P. Gast, C.K. Hall, and W.B. Russel, J. Colloid Interface Sci. **96**, 251 (1983).

[5] T. Biben and J.P. Hansen, Phys. Rev. Lett. **66**, 2215 (1991).

[6] H.N.W. Lekkerkerker, W.C.K. Poon, P.N. Pusey, A. Stroobants, and P.B. Warren, Europhys. Lett. **20**, 559 (1992).

[7] M. Dijkstra, R. van Roij, and R. Evans, Phys. Rev. Lett. **81**, 2268 (1998).

[8] J.C. Crocker and D.G. Grier, Phys. Rev. Lett. **73**, 352 (1994); **77**, 1897 (1996); K. Vondermasson, J. Bongers, A. Mueller, and H. Versmold, Langmuir **10**, 1351 (1994).

[9] H. Löwen, J.P. Hansen, and P.A. Madden, J. Chem. Phys. **98**, 3275 (1993).

[10] J.W. Verwey and J.Th.G. Overbeek, *Theory of the Stability of Lyotropic Colloids* (Elsevier, Amsterdam, 1948).

[11] G.M. Kepler and S. Fraden, Phys. Rev. Lett. **73**, 356 (1994).

[12] A.E. Larsen and D.G. Grier, Nature (London) **385**, 230 (1997).

[13] D. Goulding and J.P. Hansen, Mol. Phys. **95**, 649 (1998).

[14] N. Ise, T. Okubo, M. Sugimura, K. Ito, and H.J. Nolte, J. Chem. Phys. **78**, 536 (1983).

[15] K. Ito, H. Hiroshi, and N. Ise, Science **263**, 66 (1994); B.V.R. Tata, E. Yamahara, P.V. Rajamani, and N. Ise, Phys. Rev. Lett. **78**, 2660 (1997).

[16] B.V.R. Tata, M. Rajalakshmi, and A.K. Arora, Phys. Rev. Lett. **69**, 3778 (1992).

[17] T. Palberg and M. Würth, Phys. Rev. Lett. **72**, 786 (1994).

[18] M.J. Grimson and M. Silbert, Mol. Phys. **74**, 397 (1991).

[19] R. van Roij and J.P. Hansen, Phys. Rev. Lett. **79**, 3082 (1997).

[20] J.M. Victor and J.P. Hansen, J. Chem. Soc., Faraday Trans. 2 **81**, 43 (1985).

[21] See, e.g., N.W. Ashcroft and D. Stroud, Solid State Phys. **33**, 1 (1978).

[22] For recent reviews, see R. Evans, in *Fundamentals of Inhomogeneous Fluids*, edited by D. Henderson (Marcel Dekker, New York, 1993); or J.P. Hansen, in *Phase Transitions in Complex Fluids*, edited by M. Baus, L.F. Rull, and J.P. Rijckaert (Kluwer, Dordrecht, 1995).

[23] I. Sogami and N. Ise, J. Chem. Phys. **81**, 6320 (1984).

[24] P.B. Warren, J. Phys. II **7**, 343 (1997).

[25] See, e.g., J.P. Hansen and I.R. McDonald, *Theory of Simple Liquids*, 2nd ed. (Academic Press, London, 1986).

[26] D. Frenkel and B. Smit, *Understanding Molecular Simulations: From Algorithms to Applications* (Academic Press, Cambridge, 1996).

[27] D. Frenkel and A.C. Ladd, J. Chem. Phys. **81**, 3188 (1984).

[28] M.O. Robbins, K. Kremer, and G.S. Grest, J. Chem. Phys. **88**, 3286 (1988).

[29] J. Langmuir, J. Chem. Phys. **6**, 873 (1938).

[30] A summary of this thesis is contained in J. Michaeli, J.Th.G. Overbeek, and M.J. Voorn, J. Polym. Sci. **23**, 443 (1957).

[31] M.J. Stevens and M.O. Robbins, Europhys. Lett. **12**, 81 (1990).

[32] J.L. Barrat and J.F. Joanny, Adv. Chem. Phys. **XCIV**, 1 (1996).

[33] M. Stevens, M.L. Falk, and M.O. Robbins, J. Chem. Phys. **104**, 5209 (1996).

[34] E. Allahyarov, I. D'Amico, and H. Löwen, Phys. Rev. Lett. **81**, 1334 (1998).

[35] An excellent account of the recent work is contained in Y. Levin and M.E. Fisher, Physica A **225**, 164 (1996).

[36] C.E. Woodward, J. Chem. Phys. **89**, 5140 (1988).